

A Synoptic Map of Halo Substructures from the Pan-STARRS1 3π Survey

Edouard J. Bernard,^{1,2*} Annette M. N. Ferguson,² Edward F. Schlafly,³
 Nicolas F. Martin,^{4,5} Hans-Walter Rix,⁵ Eric F. Bell,⁶ Douglas P. Finkbeiner,^{7,8}
 Bertrand Goldman,⁵ David Martínez-Delgado,⁹ Branimir Sesar,⁵
 Rosemary F. G. Wyse,^{10,2} William S. Burgett,¹¹ Kenneth C. Chambers,¹²
 Peter W. Draper,¹³ Klaus W. Hodapp,¹² Nicholas Kaiser,¹² Rolf-Peter Kudritzki,¹²
 Eugene A. Magnier,¹² Nigel Metcalfe,¹³ Richard J. Wainscoat,¹² Christopher Waters¹²

¹ *Université Côte d'Azur, OCA, CNRS, Lagrange, France*

² *SUPA, Institute for Astronomy, University of Edinburgh, Royal Observatory, Blackford Hill, Edinburgh EH9 3HJ, UK*

³ *Lawrence Berkeley National Lab, 1 Cyclotron Road, Berkeley, CA 94720, USA*

⁴ *Observatoire Astronomique de Strasbourg, Université de Strasbourg, CNRS, UMR 7550, 11 rue de l'Université, F-67000 Strasbourg, France*

⁵ *Max-Planck-Institut für Astronomie, Königstuhl 17, D-69117 Heidelberg, Germany*

⁶ *Department of Astronomy, University of Michigan, 500 Church St., Ann Arbor, MI 48109, USA*

⁷ *Department of Physics, Harvard University, 17 Oxford Street, Cambridge, MA 02138, USA*

⁸ *Harvard-Smithsonian Center for Astrophysics, 60 Garden Street, Cambridge, MA 02138, USA*

⁹ *Astronomisches Rechen-Institut, Zentrum für Astronomie der Universität Heidelberg, Mönchhofstr. 12–14, D-69120 Heidelberg, Germany*

¹⁰ *Department of Physics and Astronomy, The Johns Hopkins University, 3400 North Charles Street, Baltimore, MD 21218, USA*

¹¹ *GMTO Corporation, 465 N. Halstead St., Suite 250, Pasadena, CA 91107, USA*

¹² *Institute for Astronomy, University of Hawaii, 2680 Woodlawn Drive, Honolulu HI 96822, USA*

¹³ *Department of Physics, Durham University, South Road, Durham DH1 3LE, UK*

Accepted 2016 August 22. Received 2016 August 19; in original form 2016 July 19

ABSTRACT

We present a panoramic map of the entire Milky Way halo north of $\delta \sim -30^\circ$ ($\sim 30,000$ deg²), constructed by applying the matched-filter technique to the Pan-STARRS1 3π Survey dataset. Using single-epoch photometry reaching to $g \sim 22$, we are sensitive to stellar substructures with heliocentric distances between 3.5 and ~ 35 kpc. We recover almost all previously-reported streams in this volume and demonstrate that several of these are significantly more extended than earlier datasets have indicated. In addition, we also report five new candidate stellar streams. One of these features appears significantly broader and more luminous than the others and is likely the remnant of a dwarf galaxy. The other four streams are consistent with a globular cluster origin, and three of these are rather short in projection ($\lesssim 10^\circ$), suggesting that streams like Ophiuchus may not be that rare. Finally, a significant number of more marginal substructures are also revealed by our analysis; many of these features can also be discerned in matched-filter maps produced by other authors from SDSS data, and hence they are very likely to be genuine. However, the extant 3π data is currently too shallow to determine their properties or produce convincing CMDs. The global view of the Milky Way provided by Pan-STARRS1 provides further evidence for the important role of both globular cluster disruption and dwarf galaxy accretion in building the Milky Way's stellar halo.

Key words: Hertzsprung-Russell and colour-magnitude diagrams – surveys – Galaxy: halo – Galaxy: structure

1 INTRODUCTION

One consequence of the hierarchical galaxy formation process predicted by cold dark matter cosmological models is that a significant fraction of the stellar mass in galaxies has

* E-mail: ebernard@oca.eu (EJB)

been accreted. In disc galaxies like the Milky Way, stars that formed *ex situ* are overall a minority, but dominate the stellar halo (e.g. Pillepich, Madau, & Mayer 2015). In these outer regions, where dynamical times are extremely long, the accreted material remains coherent for many billions of years (e.g. Johnston, Hernquist, & Bolte 1996). Stellar streams are therefore powerful probes of the formation and evolution of galaxies: in addition to providing direct evidence of past and ongoing accretion and disruption events, the observed properties of these substructures contain a wealth of information on both their progenitors and their host galaxy. For example, the stars from disrupted galaxies and globular clusters approximately follow, and therefore trace, the orbit of their progenitor, which provides an estimate of the mass and morphology of the potential enclosed within the orbit (e.g. Koposov, Rix, & Hogg 2010). The apparent width and velocity dispersion of globular cluster streams are strongly affected by density variations along their orbits, and can thus reveal the amount of clumpiness of the dark matter halo (e.g. Ibata et al. 2002; Ngan et al. 2016). Finally, Errani, Peñarrubia, & Tormen (2015) have recently shown that the dark matter profile of dwarf spheroidal galaxies plays an important role in defining the sizes and internal dynamics of their tidal streams.

With the advent of wide-field photometric observations and surveys, many streams and substructures have been detected in the Milky Way (see Grillmair & Carlin 2016, and references therein; hereafter GC16) and in nearby galaxies (e.g. Malin & Hadley 1997; Shang et al. 1998; Ibata et al. 2001; Martínez-Delgado et al. 2010; Ibata et al. 2014; Okamoto et al. 2015; Duc et al. 2015; Crnojević et al. 2016). In the Galaxy, most of the known substructures have been discovered by searching for coherent stellar over-densities in the homogeneous, wide-field photometric catalogue provided by the *Sloan Digital Sky Survey* (SDSS; York et al. 2000), although several streams have recently been found in other wide-field surveys (e.g. Bernard et al. 2014a; Koposov et al. 2014; Martin et al. 2014; Balbinot et al. 2016). While some streams have clearly originated from the accretion of dwarf galaxies, about three quarters are consistent with globular cluster disruption according to GC16. Since several teams have dedicated significant, independent efforts with the goal of detecting new substructures, one could expect that any stream within the detection limit of SDSS would have been found by now. However, like any survey, the SDSS catalogue suffers from artefacts, areas with shallower photometry due to e.g. weather conditions, and calibration issues revealing the observation patterns (see e.g. Finkbeiner et al. 2016).

Here we present a systematic search for stellar substructures in the whole sky north of $\delta > -30^\circ$ by taking advantage of the extensive coverage of the Pan-STARRS1 (PS1) 3π Survey. It significantly expands on the previous Milky Way substructure work that was carried out with an earlier data processing version of PS1 (Slater et al. 2013, 2014; Bernard et al. 2014b; Morganson et al. 2016). The current processing version reaches to roughly the same depth as the SDSS but covers $30,000 \text{ deg}^2$ with homogeneous and well-calibrated photometry. The observational strategy and data reduction procedure are completely different from those of SDSS, thereby allowing a fully independent analysis. We first provide a summary of the substructures recovered in

our analysis, including further extensions of known features, then present five new candidate streams, all but one of which lie within the SDSS footprint.

2 THE PAN-STARRS1 3π SURVEY

This work is based on the current internal data release of the PS1 3π Survey (Processing Version 3; K. C. Chambers et al., in preparation), which covers the whole sky visible from Hawaii in five bands (Dec. $\gtrsim -30^\circ$; $g_{P1}r_{P1}i_{P1}z_{P1}y_{P1}$, hereafter *grizy*). The current depth of the catalogue, based on single-epoch photometry, reaches $g \sim 22$ with a signal-to-noise ratio of 5. This corresponds to the old main-sequence turn-off (MSTO) magnitude of a stellar population at a heliocentric distance of ~ 35 kpc, and thus probes a significant fraction of the Milky Way stellar halo.

The PS1 catalogue used in this paper is maintained by one of the authors (EFS) and stored in the Large Survey Database (LSD) format (Juric 2012), which allows for a fast and efficient manipulation of very large catalogues ($> 10^9$ objects). It contains both the point-spread function (PSF) and aperture photometry of each object, the difference between the two providing a convenient parameter to separate stars and background galaxies (see below).

3 DATA ANALYSIS

Our search for halo substructures in the 3π dataset is based on the application of the matched-filter technique (Rockosi et al. 2002). In creating stellar density maps, this method gives higher weight to stars that are more likely to belong to an old and metal-poor (OMP; i.e. potentially accreted) component than to the main field population. The filter is built as the ratio of the Hess diagram of a OMP population to the Hess diagram of the field stars. The convolution is repeated by shifting the filter in magnitude to probe a range of heliocentric distances.

The matched-filter algorithm used here is based on the description of Odenkirchen et al. (2003). It was written by one of us (EJB) as a MapReduce kernel for LSD to take advantage of the highly efficient, parallelized framework of LSD. This efficiency allowed us to carry out the matched-filtering over the whole PS1 footprint in a single run (i.e. $\sim 30,000 \text{ deg}^2$), and to experiment with many different combinations of age, metallicity, heliocentric distance, and photometric bands in constructing the optimal filter.

While many studies to date have used the CMD of the globular cluster M13 (NGC 6205; e.g. Grillmair 2009; Bonaca, Geha, & Kallivayalil 2012) to build the filter, we have chosen to use synthetic colour-magnitude diagrams (CMDs). This implementation has several advantages: (i) we can generate arbitrarily well populated CMDs at all magnitudes; (ii) these CMDs are not contaminated by field objects; (iii) we can simulate photometric uncertainties adequately for all distances probed without having first to correct for the actual uncertainties of the M13 observations; and (iv) we can repeat the convolution with different combinations of ages and metallicities. The synthetic CMDs were generated from

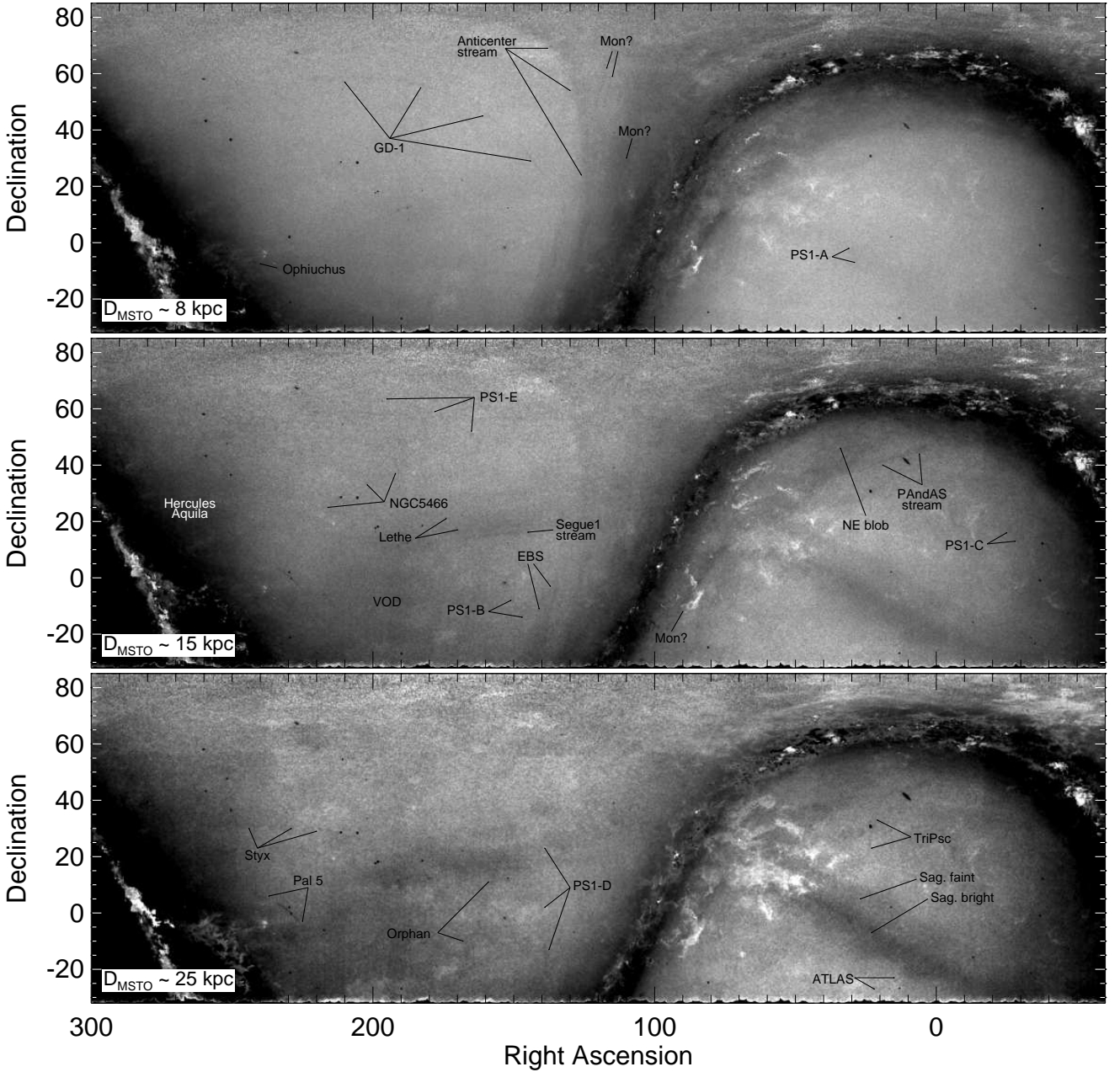


Figure 1. Matched-filtered stellar density maps of the whole PS1 footprint. The stretch is logarithmic, with darker areas indicating higher surface densities; a few black patches are due to missing data. The top, middle, and bottom panels correspond broadly to heliocentric distances of 8.5, 15, and 25 kpc. The main substructures are labeled and discussed in Section 4; new candidate streams (labelled PS1-A to E) are presented in Section 5.

PARSEC isochrones (Bressan et al. 2012) in the PS1 bands¹ following the luminosity function provided in the isochrone files, and corrected for completeness as a function of magnitude as measured in the representative region described below. In contrast, the field Hess diagram was produced empirically by selecting all the stellar objects within the region

¹ downloaded from version 2.8 of <http://stev.oapd.inaf.it/cgi-bin/cmd>

defined by $215^\circ < RA < 245^\circ$ and $15^\circ < Dec. < 60^\circ$, corresponding to an area of 10^3 deg^2 containing $\sim 4.9 \times 10^6$ objects. This region was chosen because it does not contain any known Local Group dwarf galaxy or globular cluster. In addition, as it encompasses a wide range of Galactic latitudes, it is representative of the field population over most of the sky where substructures are likely to be detected with this method.

Only stellar-like objects (i.e. defined as $|r_{\text{PSF}} -$

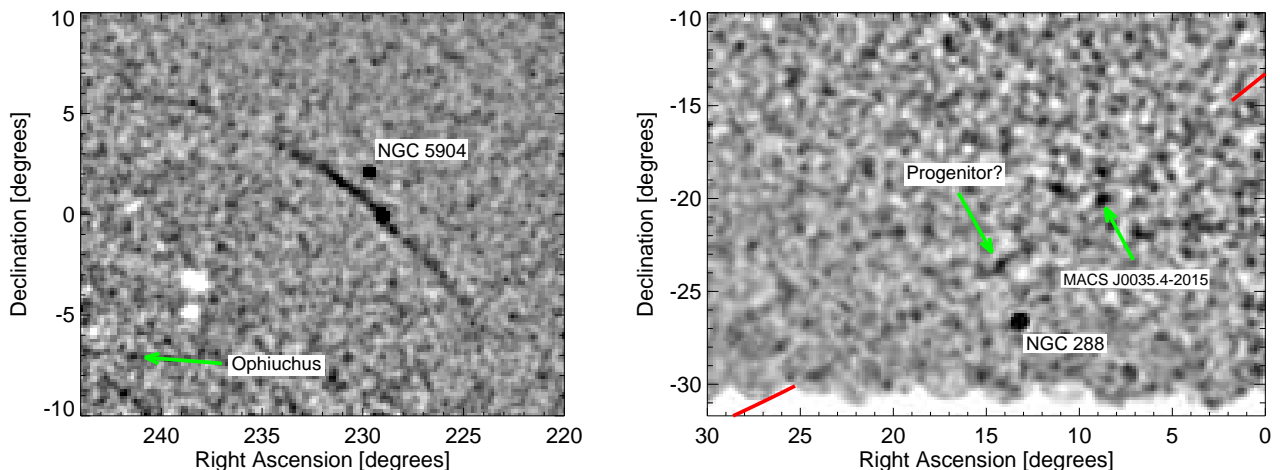


Figure 2. Close-up view of the area around Pal 5 (left) and the ATLAS stream (right). To remove large-scale background variations, the maps were smoothed with a Gaussian kernel of width 2° and subtracted from the original maps. Some fore- and background features are labeled. The red line in the right panel shows the best fitting great circle containing the stream, with north pole at $(\alpha, \delta)=(74^\circ 599, 48^\circ 365)$.

$r_{\text{aperture}}| \leq 0.2$) with photometric uncertainties below 0.2 mag in either (g and r) or (g and i) were taken into account. They were then corrected for foreground reddening by interpolating the extinction at the position of each source using the Schlafly et al. (2014) dust maps with the extinction coefficients of Schlafly & Finkbeiner (2011). The matched-filtering was carried out in 26 heliocentric distance slices from 3.5 to 35 kpc (i.e. distance moduli from 12.7 to 17.7 separated by 0.2 mag) in both ($g-r, g$) and ($g-i, g$) filter combinations. After visual examination of the different slices, we decided to coadd slices 8 to 13, 14 to 19, and 20 to 25, to produce three maps for each filter combination, corresponding broadly to heliocentric distances of $\sim 8.5, 15,$ and 25 kpc. Finally, we corrected for the different pixel area over the sky for better contrast at high declination, and averaged the ($g-r, g$) and ($g-i, g$) maps together to produce the maps shown in Fig. 1. The pixel scale is $5'$, smoothed by a Gaussian kernel with a full-width at half-maximum (FWHM) of 3 pixels for the 8.5 and 15 kpc maps, and 4 pixels for the 25 kpc map. We found this angular resolution to be the best compromise between revealing the broad, diffuse substructures and smoothing out the cold streams. Note, however, that some features (e.g. PS1-E, see below) are much more prominent when using a broader Gaussian filter.

We repeated the filtering for different combinations of age (8, 10, 12, and 13.5 Gyrs) and metallicity ($[\text{Fe}/\text{H}] = -2.2, -1.9, -1.5, -1.0$), but found that (12, -1.5) produced the best overall contrast. The FITS file containing the 26 distance slices from 3.5 to 35 kpc based on that age/metallicity combination, and a second file with the three coadded, unsmoothed maps used to create Fig. 1, are made available online².

4 RECOVERY OF KNOWN SUBSTRUCTURES

The majority of known stellar streams and substructures have been discovered thanks to the *Sloan Digital Sky Sur-*

vey (SDSS; York et al. 2000), which observed roughly 14,555 square degrees of sky at a comparable depth to the PS1 3π survey. This area is completely contained within the PS1 footprint and hence our ability to recover these features provides a check on the photometric accuracy and purity of the current catalogue. As a reference database, we use the recent compilation of Milky Way halo streams presented by GC16 and complement this with additional features which have been subsequently discovered by Balbinot et al. (2016) and Belokurov & Koposov (2016) using data from the *Dark Energy Survey* (DES; The Dark Energy Survey Collaboration 2005).

Our maps clearly reveal all the prominent structures that have been reported, but also most of the fainter detections. In particular, we recover the bright and faint streams from the Sagittarius dwarf galaxy (Ibata, Gilmore, & Irwin 1994; Belokurov et al. 2006b), the tails of Palomar 5 (Odenkirchen et al. 2001), the Orphan stream (Belokurov et al. 2006b; Grillmair 2006a), GD-1 (Grillmair & Dionatos 2006b), the Anticentre stream and the Eastern Banded Structure (EBS; Grillmair 2006b), the ATLAS stream (Koposov et al. 2014), the Pisces-Triangulum stream (Bonaca, Geha, & Kallivayalil 2012), the Ophiuchus stream (Bernard et al. 2014a), the PAndAS MW stream and the PAndAS northeast blob (Martin et al. 2014), the tidal feature around Segue 1 (Niederste-Ostholt et al. 2009), the Hercules-Aquila cloud (Belokurov et al. 2007a), and the Virgo Overdensity (VOD Ivezić et al. 2000). These features are labelled in the map of their corresponding distance slice as shown in Fig. 1. A close examination of the maps in FITS format also reveals the tails of NGC 5466 (Belokurov et al. 2006a), as well as portions of Lethe and Styx (Grillmair 2009), and Hyllus and Hermus (Grillmair 2014a).

On the other hand, there are a few features listed in the GC16 compilation that we do not recover – namely, the Virgo Stellar stream (VSS; Duffau et al. 2006), Acheron and Cocytos (Grillmair 2009), the Cetus Polar stream (CPS; Newberg, Yanny, & Willett 2009), the Pisces overdensity (POD; Sesar et al. 2007), and TriAnd (Majewski et al. 2004;

² <http://dx.doi.org/10.5281/zenodo.60518>

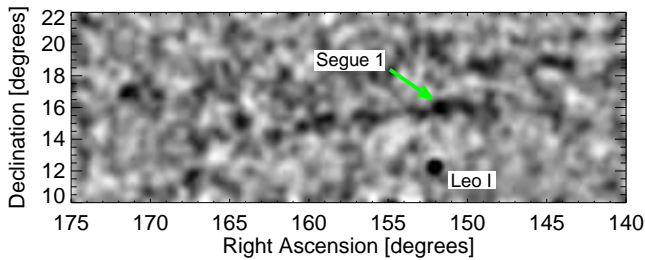


Figure 3. Same as Figure 2 for the stream in the vicinity of Segue 1, which extends from R.A. of $\sim 144^\circ$ to 168° .

Martin, Ibata, & Irwin 2007). However, in most of these cases, the absence of these features in our maps is understandable: we note that both the VSS and CPS are broad and diffuse streams that have not yet been observed in matched-filter or MSTO maps, the POD lies more than twice as far away as the reach of our photometry, and Acheron and Cocytos are located in a dense stellar region near the bulge, which complicates their detection. While we do not observe any well-defined overdensities that could correspond to TriAnd, we note that the middle and bottom panels of Fig. 1 do reveal low-level diffuse structure in the vicinity of the Andromeda galaxy. In summary, we believe that there are good reasons why these specific features will not be visible in PS1 and emphasize the excellent overall recovery rate we have achieved for known streams over this large swath of the sky.

Four stellar streams have been discovered to date that lie outside the PS1 footprint (at $\delta < -30^\circ$), namely Alpheus (Grillmair et al. 2013), streams S2 and S3 (Belokurov & Koposov 2016), and Phoenix (Balbinot et al. 2016). It has recently been argued that the latter may be an extension of the Hermus stream (Grillmair 2014a; Grillmair & Carlberg 2016). Based on their known trajectories, we conducted a search for possible extensions of all these streams in the PS1 footprint, but did not find any significant overdensities. That said, both S2 and S3 have heliocentric distances larger than 50 kpc and are therefore also beyond the volume sampled here.

In several cases, the PS1 data provide new constraints on the properties and/or spatial extension of known streams. In the following subsections, we discuss a number of the specific features. Note that Sagittarius and Monoceros have already been discussed extensively in the context of the PS1 data (Slater et al. 2013, 2014; Hernitschek et al. 2016; Morganson et al. 2016).

4.1 The tidal tails of Palomar 5

The Galactic globular cluster Palomar 5 (Pal 5) harbors the most prominent tidal tails among the known Milky Way clusters, and naturally these have been extensively studied. The tails were first discovered by Odenkirchen et al. (2001) using small area SDSS commissioning data, but subsequent SDSS data releases with expanding coverage allowed them to be traced far further. The currently known length of the Pal 5 stream is $\sim 22^\circ$ on the sky (Grillmair & Dionatos 2006a), though it is truncated in the south by the edge of the SDSS survey at $\delta = -2.5^\circ$.

While there have been numerous observational efforts to obtain deeper photometric data (e.g. Ibata, Lewis, & Martin 2016), as well as spectroscopic measurements (e.g. Odenkirchen et al. 2009), to constrain the properties and possible orbits of the stream, these have focused on the portion of the stream which lies inside the SDSS footprint. With a spatial coverage extending about 30° further to the south, PS1 allows us to search for extensions of the stream beyond this area. From our maps (see Figure 2), we are able to trace the Pal 5 stream further south to $\delta = -6^\circ$, where it appears to end abruptly. This is not an observational bias due to e.g. a distance gradient along the stream, since in that case we would expect to see the stream appear in nearer/more-distant slices. This means that the leading ($\sim 8^\circ$) and trailing ($\sim 15^\circ$) tails of Pal 5 are of distinctly different traceable angular extent.

4.2 The ATLAS stream

The ATLAS stream was recently discovered by Koposov et al. (2014) from early data of the ATLAS survey (Shanks et al. 2015). They were able to trace it over 12° , from $\delta \sim -32^\circ$ to the edge of a gap in the spatial coverage at the time at $\delta = -25^\circ$; there appeared to be no continuation of this feature in the narrow ATLAS stripe covering $-13.5^\circ < \delta < -10^\circ$. In our maps – zoom-in map is shown in Figure 2 – we find that the stream extends significantly further north to about $\delta = -15^\circ$. It therefore appears that the combination of the ATLAS and PS1 surveys covers the entire $\sim 28^\circ$ length of this stream.

The narrow width of the stream (~ 0.25 deg) combined with the metal-poor nature of its stellar population led to Koposov et al. (2014) to conclude that the progenitor was a globular cluster. A compact overdensity is visible in Fig. 1 along the stream at $(\alpha, \delta) \sim (0^h 35^m, -20^\circ 05^m)$. However, inspection of the stacked images reveals a background galaxy cluster (MACS J0035.4-2015) is most likely responsible for this enhancement. Aside from this, there is also a significant, broader overdensity at $(\alpha, \delta) \sim (0^h 57^m, -23^\circ 29^m)$, which roughly coincides with the centre of the stream. Interestingly, the matched-filter maps suggest this feature has an – admittedly low significance – S-shaped morphology, as would be expected for a disrupting globular cluster. There is no obvious stellar concentration visible at this position in the stacked images and hence deeper imaging will be necessary to confirm its presence.

Based on simple orbit modelling, Koposov et al. (2014) suggested that a possible progenitor of the ATLAS stream might be the sparse halo globular cluster Pyxis. Pyxis lies at $(\alpha, \delta) \sim (9^h 08^m, -37^\circ 13^m)$ and hence outwith the PS1 footprint. Although we cannot directly test this association with our data, our detections of the stream at more northern latitudes will enable significantly improved constraints on possible progenitor orbits.

4.3 The stream in the vicinity of Segue 1

Based on an analysis of SDSS data, Niederste-Ostholt et al. (2009) report tidal tails extending to $\sim 1^\circ$ both eastward and southwest of Segue 1. A matched-filter analysis of the same data by Grillmair (2014b) suggests that this field con-

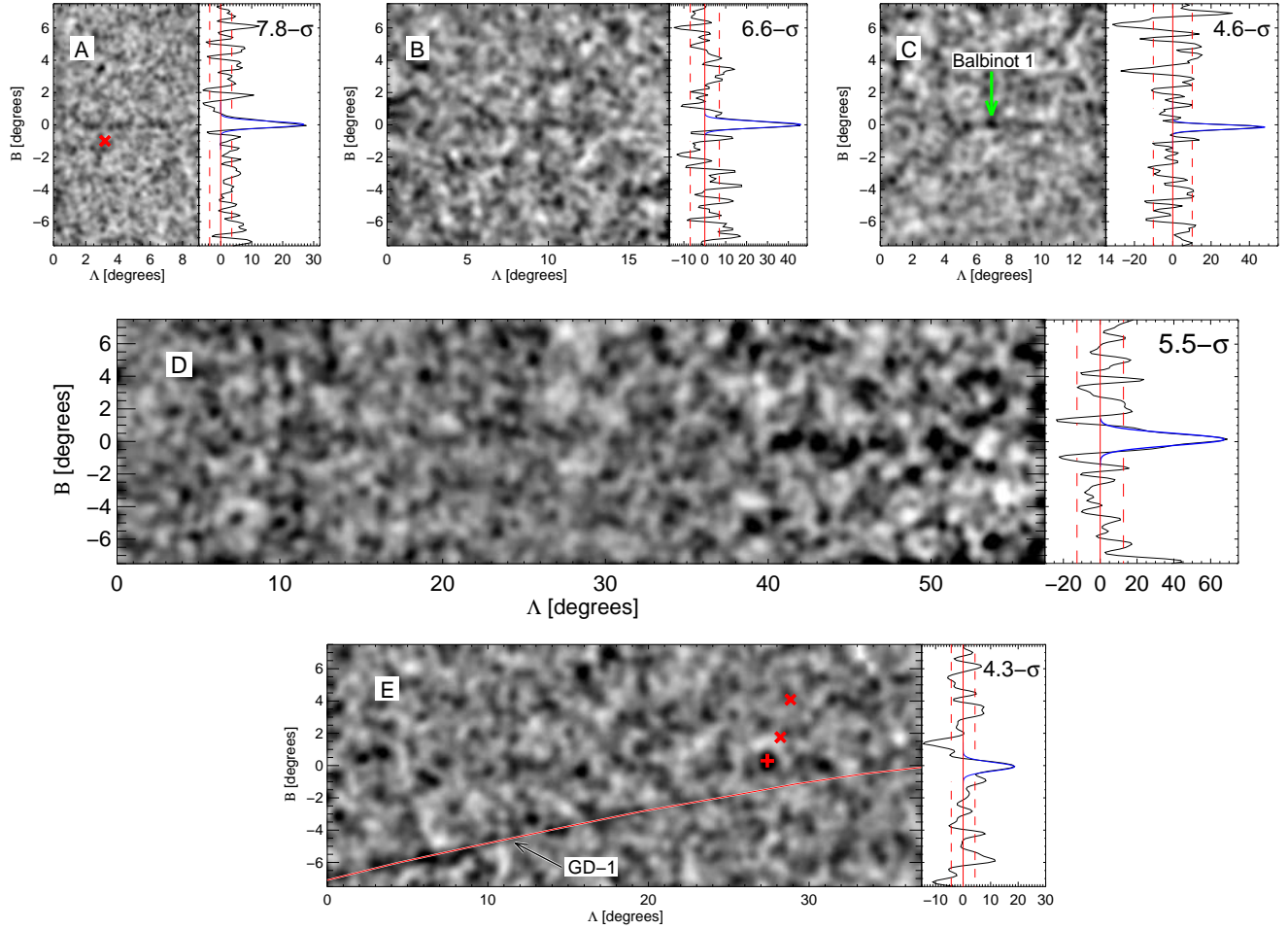


Figure 4. Close-up view of the new stream candidates. For each stream, we show the matched-filtered map in the coordinate system of the stream (*left*) and the average stellar density projected onto the B axis in arbitrary units (*right*, *see text*). In the maps, which are the coaddition of the four distance slices in which the stream signal is strongest, the streams lie at $B \sim 0$ with the right hand side being the southern-most point. In the cross-section panels, the dashed lines show the $1\text{-}\sigma$ dispersion of the background, while the blue line is a Gaussian fit to the stream profile. The significance of detection is also indicated. *PS1-A*: The red cross in the left panel shows the Galactic globular cluster Whiting 1, which is unrelated to the stream. *PS1-C*: Even after masking a 1 deg^2 area around Balbinot 1 – at $(\Lambda, B) \sim (7, 0)$ – the peak of *PS1-C* still reaches $4.1\text{-}\sigma$. *PS1-D*: The peak of the profile is at $4.8\text{-}\sigma$, or $3.4\text{-}\sigma$ for $\Lambda < 40^\circ$. *PS1-E*: The peak of the profile is at $4.3\text{-}\sigma$ when masking a 1 deg^2 area around the overdensity marked with a plus sign at $(\Lambda, B) \sim (27.5, 0.4)$. The cross symbols represent Willman 1 (lower; Willman et al. 2005a) and Ursa Major I (upper; Willman et al. 2005b). The narrow stream highlighted in red is GD-1.

tains a narrow stream extending over at least 25° , but lying a few kpc closer than Segue 1. Follow-up spectroscopic analysis of this region (Geha et al. 2009; Norris et al. 2010; Simon et al. 2011) led to the detection of a cold component with $v_{helio} \sim 300\text{ km s}^{-1}$ having stellar population and heliocentric distance roughly comparable to those of Segue 1, but significantly offset in radial velocity. Unfortunately, the spectroscopic observations only cover a small area around Segue 1, so it is not clear yet how the tidal extensions, the 25° stream and the 300 km s^{-1} velocity component are connected. The region around Segue 1 is further complicated by the fact that the Sagittarius stream lies in the background and may possess a component with such a radial velocity.

Inspection of our maps recovers a $\sim 24^\circ$ stream crossing Segue 1 (see Figure 3). Consistent with Grillmair (2014b), we find this feature lies several kpc closer than Segue 1 which is at a heliocentric distance of $\sim 23\text{ kpc}$. There appears to be

a distance gradient along the stream with the eastern end closer to the Sun than the western end ($\sim 14\text{ kpc}$ vs. $\sim 19\text{ kpc}$). This gradient is opposite to that of the Sagittarius Stream in the same longitude range (e.g. Belokurov et al. 2006b), which further strengthens the case of the stream being separate from both Segue 1 and Sagittarius (e.g. Frebel et al. 2013). Confirmation of the association with the 300 km s^{-1} population will require spectroscopic observations of stream members several degrees away from Segue 1.

4.4 Monoceros and the anticentre substructures

The Milky Way disc in the direction of the anticentre contains a number of features whose nature and origin are still hotly debated (see Slater et al. 2014; Morganson et al. 2016, for a detailed description and historical review). This low-latitude substructure is often referred to as the Monoceros

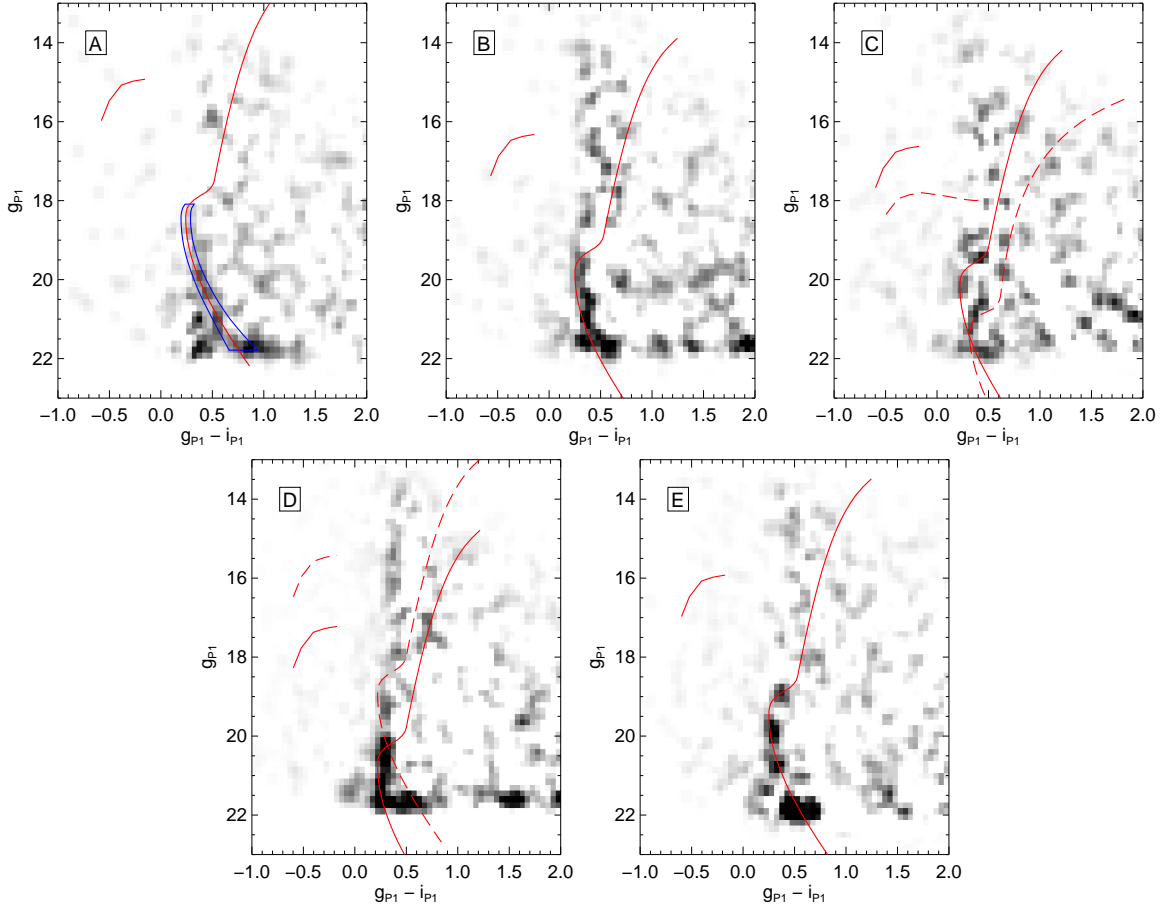


Figure 5. Extinction-corrected CMDs of the new stream candidates. The red lines are globular cluster fiducials from Bernard et al. (2014b), shifted to the distance obtained from the matched-filtered slices where the signal of the streams was stronger. The dashed fiducials in panels C and D correspond to other substructures in the line of sight, complicating the CMDs: Balbinot 1 and the EBS, respectively. Balbinot 1 is represented by the fiducial of M3, while the fiducial of M92 is used for the other features. In panel A, the blue polygon represents the selection box used to select stream member stars for the significance and width measurements; similar boxes have been used for each stream, adapted to their distance and photometric uncertainties.

Ring, after the constellation in which the first evidence was discovered. It forms a large and complex stellar enhancement in the outer disc, mainly confined between 14–18 kpc from the Galactic centre, and extending from $120^\circ < l < 240^\circ$ and $-30^\circ < b < +40^\circ$. It is most visible in the top panel of Figure 1 between RA of ~ 110 and -20° and on either sides of the disc. It has a rather sharp edge, as might be expected from a flaring of the outer disc. Recent work has shown that these low-latitude features could primarily be the result of disc oscillations (Xu et al. 2015), possibly as a consequence of a low-mass satellite fly-by (e.g. Gómez et al. 2016).

In our maps, several new, well-defined substructures in the anticentre region can be identified and we label these ‘Mon?’, as it is unclear if and how they are related to Monoceros. For example, the two parallel marks labeled ‘Mon?’ in the top panel of Figure 1 lie within 2° of the EBS orbit projections from Grillmair, Carlin, & Majewski (2008), and may therefore be an extension of this feature.

There is also a broad component at $(\alpha, \delta) \sim (80^\circ, 0^\circ)$, running parallel to the Milky Way disc, labelled ‘Mon?’ in the middle panel. In the top panel it appears to be part of the disc flaring (although with a sharper southwest edge), but it is still clearly visible in the other two panels where

the disc flaring feature has faded. We have checked that the appearance of this feature is not an effect of the reddening in this part of the sky by comparison with the dust maps from Schlafly et al. (2014). It is intriguing that Fig. 13 of Morganson et al. (2016), which presents the heliocentric distance to the Monoceros Ring centre of mass along each line of sight, shows a clear feature with a similar shape at the same location; it is distinguished by being located roughly 5 kpc further away than the surrounding stars. Further observations will be required before it can be established if this feature is merely part of the perturbed Milky Way outer disc or an accreted component.

4.5 The Orphan stream

The Orphan stream, so named for its lack of an obvious progenitor, was independently discovered in SDSS survey data by Belokurov et al. (2006b) and Grillmair (2006a), who mapped it over more than 60° on the sky. With a width of 2° and a significant internal metallicity dispersion, it is most likely the result of the tidal disruption of a dwarf galaxy. Grillmair et al. (2015) recently used the DECam on

Table 1. Summary of the Properties of the Newly-Discovered Candidate Streams.

Parameter	PS1-A	PS1-B	PS1-C	PS1-D	PS1-E
R.A. (J2000.0)	01:57:02	09:53:15	22:10:28	09:19:26	11:33:20
Dec. (J2000.0)	-04:14:34	-11:07:22	+14:56:29	+00:50:14	+55:23:27
l	160° 17	248° 41	75° 12	231° 06	144° 17
b	-62° 27	+32° 30	-32° 60	+32° 83	58° 40
$(m-M)_0$	14.5 ± 0.5	15.8 ± 0.5	16.2 ± 0.5	16.8 ± 0.5	15.5 ± 0.5
Median E(B-V)	0.03	0.06	0.10	0.05	0.02
Heliocentric distance	7.9 ^{+2.1} _{-1.6} kpc	14.5 ^{+3.7} _{-3.0} kpc	17.4 ^{+4.5} _{-3.6} kpc	22.9 ^{+5.9} _{-4.7} kpc	12.6 ^{+3.3} _{-2.6} kpc
Width (FWHM)	27' ± 3' (63 ± 7 pc)	27' ± 3' (112 ± 14 pc)	20' ± 4' (99 ± 20 pc)	52' ± 6' (350 ± 40 pc)	37' ± 6' (140 ± 20 pc)
Length	~ 5° (~ 700 pc)	~ 10° (~ 2.5 kpc)	~ 8° (~ 2.4 kpc)	~ 45° (~ 21 kpc)	~ 25° (~ 5.5 kpc)
M_V	-1.0 ^{+0.5} _{-0.7}	-2.8 ^{+0.3} _{-0.5}	-2.7 ^{+0.4} _{-0.6}	-4.9 ^{+0.2} _{-0.3}	-1.9 ^{+0.4} _{-0.6}
L_V	0.22 ^{+0.19} _{-0.08} × 10 ³ L _⊙	1.2 ^{+0.8} _{-0.3} × 10 ³ L _⊙	1.0 ^{+0.7} _{-0.3} × 10 ³ L _⊙	7.5 ^{+2.0} _{-1.3} × 10 ³ L _⊙	0.50 ^{+0.40} _{-0.15} × 10 ³ L _⊙
Pole (α, δ)	(300° 856, 20° 732)	(65° 603, 32° 567)	(232° 227, 33° 838)	(49° 640, 2° 467)	(42° 526, 23° 987)
Detection significance	7.8- σ	6.6- σ	4.6- σ	5.5- σ	4.3- σ

the Blanco telescope to trace the Orphan stream beyond the southern edge of the SDSS footprint. In addition to mapping the stream a further $\sim 50^\circ$, they find a moderate overdensity of stars at $\delta \sim -14^\circ$ that they suggest could be consistent with the progenitor remnant. Our maps do not reveal any clear enhancement of star counts at this location, although this part of the sky suffered from non-optimal observing conditions in the PS1 dataset. The only significant overdensity we can detect in the stream is located at $(\alpha, \delta) \sim (11^h 16^m, -22^\circ 48^m)$. This is also visible on the map of Grillmair et al. (2015), although with a lower significance. A visual inspection of the stacked images did not reveal any obvious overdensity of sources at this location.

5 NEW CANDIDATE STREAMS

Our success in recovering almost all known streams within 35 kpc that fall in the PS1 3π Survey footprint demonstrates the high quality of the photometric catalogue and it is therefore natural to conduct a search for additional, previously-unknown substructures in this area. Based on visual inspection of our maps, we have identified several other stream candidates at various distances; the five most significant detections, for which we could make convincing plots, are labelled PS1-A to E in Figure 1. We also show cropped maps, reprojected in the coordinate system of the streams, in the left hand panels of Figure 4. The corresponding CMDs made by selecting stars in a narrow box running the whole length of the stream, corrected for extinction and foreground contamination, are shown in Figure 5. The fiducial of Milky Way globular cluster M92 (NGC 6341; [Fe/H]=-2.3) from Bernard et al. (2014b) provides a good match to the observed MSTO of the candidate streams and is overplotted, while we have used the fiducial of M3 (NGC 5272; [Fe/H]=-1.5) for Balbinot 1 in panel C to match the estimated metallicity of this cluster (Balbinot et al. 2013). Note that the distance used to shift the fiducials was obtained from the matched-filter slice in which the stream signal was strongest, rather than from a fit to the CMD features. Because of the crudeness of the method used to estimate the distance and the considerable uncertainties on the age and metallicity of the stream stellar populations, we adopt a distance uncertainty of 0.5 mag.

We assessed the significance of the stream detections by using the stellar density maps, rather than the matched-filter maps in which noise can be misleading due to the amplification of stars in certain CMD positions. We began by constructing, for each stream, a colour-magnitude selection box based on the shape of the fiducial and taking into account the photometric uncertainties as a function of magnitude, as shown in the top left panel of Figure 5. The stars in this box were then used to create a spatial density map with a pixel scale of 6', smoothed with a Gaussian filter of FWHM = 2.5 pixels, which was then projected onto the latitude axis to produce a cross-section of the stream. These are shown in the right hand panels of Figure 4. The significance, defined as the peak detection, is typically 4- to 8- σ above the background noise level. The blue line is a Gaussian fit to the overdensity, from which we estimate the width and luminosity of each stream (see below). We discuss these in more detail below, and summarize the stream properties in Table 1.

We follow a method similar to that presented in Bernard et al. (2014a) to estimate the total luminosity of the streams. Firstly, IAC-STAR (Aparicio & Gallart 2004) is used to generate the CMD of an OMP population (11.5–12.5 Gyr, [Fe/H]=-2.2) with the Padova library (Girardi et al. 2000), adopting a binary fraction of 15%, typical of the observed fraction in globular clusters (e.g. Sollima et al. 2007). The CMD contains 10⁶ stars down to $M_V = 7$ (i.e. ~ 3.5 mag below the MSTO) – stars fainter than this limit have a negligible contribution to the total magnitude. The Gaussian fits to the cross-sections described above provide the excess number N of stars within the colour-magnitude selection box over the background level. We then extract stars randomly from the synthetic CMD until the selection box contains $N \pm \sigma_N$ stars, and sum their luminosity to obtain the total flux. We repeated this step 10⁴ times to take into account the effect of stochastic sampling of the CMDs; the total magnitude and luminosity of each stream are listed in Table 1.

5.1 PS1-A

PS1-A appears as a prominent, elongated overdensity in the top panel of Figure 1, projected on the southern extension of the Sagittarius bright stream. It passes within 1° of the

Milky Way globular cluster Whiting1, but is four times nearer (7.9 vs. 31.6 kpc; e.g. Carraro, Zinn, & Moni Bidin 2007) and therefore unrelated. Thanks to its proximity, it also has the most significant detection signal at 7.8σ . From the matched-filter map shown in Figure 4, we estimate a projected length of $\sim 5^\circ$, while the Gaussian fit to the cross-section profile indicates a width of $27'$. These correspond to 700 and 63 pc, respectively, at the distance of the stream. This width is comparable to the values measured for other streams resulting from the disruption of globular clusters (~ 100 pc; see e.g. Grillmair 2009; Koposov, Rix, & Hogg 2010). No obvious progenitor is visible on the maps.

5.2 PS1-B

PS1-B was found in the intermediate distance map, near the eastern edge of the EBS, where we are able to trace it over $\sim 10^\circ$. However, as shown in the middle panel of Fig. 1, it lies very close to the expected extension of the Lethe stream (Grillmair 2009); the heliocentric distances and width – ~ 14.5 kpc and 112 pc vs. 13 kpc and 95 pc for Lethe (Grillmair 2009) – are also in good agreement given our uncertainties. If these two features are indeed linked, this would constitute one of the longest globular cluster streams known ($\sim 120^\circ$).

5.3 PS1-C

PS1-C stretches for $\sim 8^\circ$ across the southern Galactic cap. With a width of 99 ± 20 pc, it is consistent with a globular cluster progenitor. Interestingly, it is roughly centred on the recently discovered globular cluster Balbinot 1 (Balbinot et al. 2013), suggesting it could represent tidal tails from this faint ($M_V = -1.21 \pm 0.66$), extended cluster. However, the approximate distance we estimate for the stream, based on the matched-filter slice in which the signal was strongest, is approximately 15 kpc, while the cluster lies at a distance of $31.9^{+1.0}_{-1.6}$ kpc (Balbinot et al. 2013). This implies that either the two features are unrelated, or that our distance is strongly under-estimated. Unfortunately, the CMD features (Figure 5) are not prominent enough to refine our estimate through isochrone fitting hence further observations are required. Note, however, that this stream is also visible as a low significance overdensity in the maps of Bonaca, Geha, & Kallivayalil (2012) based on SDSS data (see section 6), giving further credence to its reality. If the stream can be proven to be physically associated with Balbinot 1, it would contain roughly four times the luminosity of cluster, suggesting we are witnessing the object in the final throes of tidal disruption.

5.4 PS1-D

Compared to the other newly detected streams, PS1-D is significantly longer, broader, more luminous, and further away. In our maps, we trace it over 45° in projection, at a distance of about 23 kpc. At this distance, the stream is 21 kpc long and 350 pc wide, i.e. a factor ~ 3 broader than the other candidates described here. This suggests that the progenitor was a low-luminosity dwarf galaxy rather than a globular cluster (e.g. GD-1: ~ 80 pc, Koposov, Rix, & Hogg 2010 vs.

Orphan: ~ 650 pc, Belokurov et al. 2007b). The CMD shown in Figure 5 is complicated by the presence of other substructures along the same line of sight, namely the EBS, which is located at a heliocentric distance of about 10 kpc, hence the offset of ~ 1.8 mag.

5.5 PS1-E

PS1-E is the most diffuse of the streams presented here, and also has the lowest significance at 4.3σ . However, its CMD is very clean, with a well defined MSTO. As for PS1-A–C, the width of 140 ± 20 pc suggests a globular cluster origin. It runs over 25° -long, just a few degrees north of GD-1, which is also visible in Figure 4. In this plot, the overdensity at $(\Lambda, B) \sim (27.5, 0.4)$ appears to be unrelated as it is offset by $\sim 0.5^\circ$ from the stream path, so this region has been masked before calculating the stream significance and its profile. Finally, we note that the densest parts of PS1-E are also visible in the maps of Bonaca, Geha, & Kallivayalil (2012), which strongly suggests that this feature, while having a low significance, is not an artefact.

6 DISCUSSION AND CONCLUSIONS

We have presented a synoptic map of Galactic halo substructures in the sky north of $\delta \sim -30^\circ$ through applying the matched-filtering technique to the extant PS1 3π Survey dataset. Covering roughly 30,000 square degrees, this is the largest deep contiguous view of the Milky Way halo yet constructed. We have recovered almost all the previously-known stellar streams and other substructures within the volume to which we are sensitive, demonstrating the high quality and uniformity of the PS1 photometry. In addition, we have also uncovered five new candidate halo streams, one or two of which may be possible extensions of known streams and objects. Four of these streams have properties consistent with disrupting or disrupted globular clusters, while the fifth likely originates from an accreted dwarf galaxy. Three of the globular cluster streams are short in projection, subtending $\lesssim 10^\circ$ on the sky. Prior to this work, the only short GC stream known was Ophiuchus, subtending a mere 2.5° on the sky. Subsequent work has shown that Ophiuchus is likely highly foreshortened due to its inclination with our line-of-sight, but is still only ~ 1.6 kpc after deprojection (Sesar et al. 2015). The fact we have uncovered three similar examples of short streams in our full 3π analysis suggests that such features may not be that rare.

Perhaps surprisingly, four of the five new streams are located within the SDSS footprint, an area that has been thoroughly searched by several groups using similar techniques to our own (e.g. Newberg et al. 2002; Odenkirchen et al. 2003; Grillmair & Dionatos 2006b; Belokurov et al. 2007b; Bonaca, Geha, & Kallivayalil 2012). In fact, PS1-A, C, and E, and the northern end of PS1-D, are in hindsight discernable as extended overdensities in the SDSS maps of Bonaca, Geha, & Kallivayalil (2012)³, although with a much lower significance than the PscTri stream that is the subject

³ available at <http://www.astro.yale.edu/abonaca/research/halo.html>

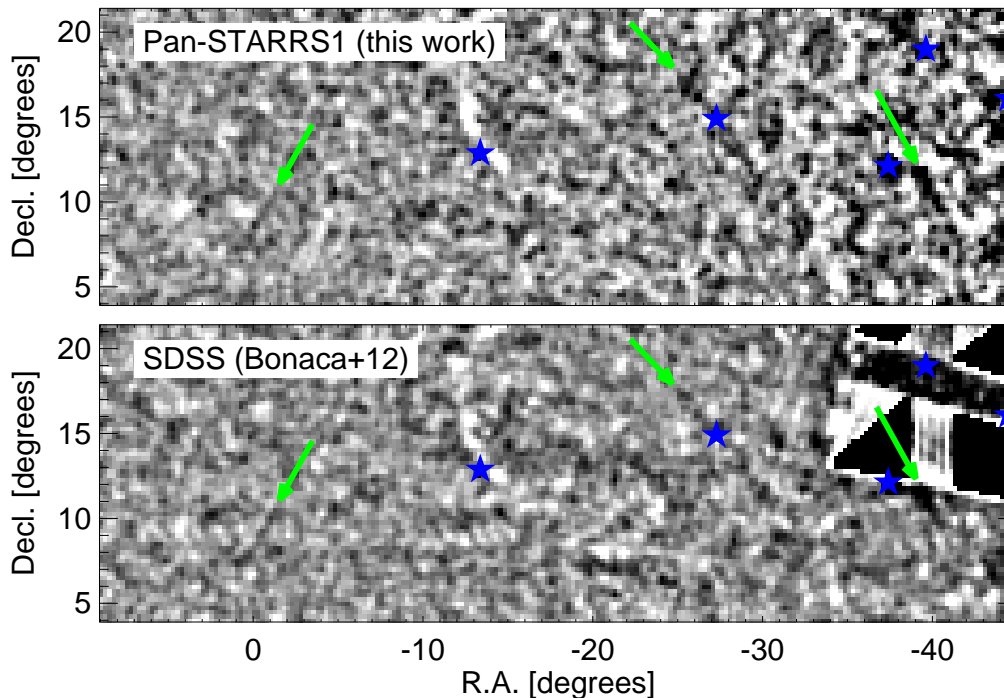


Figure 6. Comparison of our matched-filtered stellar density map at ~ 15 kpc with that obtained by [Bonaca, Geha, & Kallivayalil \(2012\)](#) from SDSS data, centred on a small patch of the south galactic cap. Blue stars show the location of known globular clusters, while the arrows point toward some of the stream-like features that are common in both maps. The width of the smoothing kernel has been chosen to highlight very narrow stream-like features; the arrow at R.A. $\sim -24^\circ$ points to PS1-C, which is more prominent with a broader smoothing kernel.

of their paper. We therefore explored the possibility of finding other low significance streams by blinking our PS1 maps with those of [Bonaca, Geha, & Kallivayalil \(2012\)](#), who used comparable distance bins. Remarkably, this process reveals many narrow, stream-like features in common, sometimes extending over tens of degrees. It also reveals compact overdensities which do not correspond to known globular clusters or dwarf galaxies, although many of those may be due to the presence of background galaxy clusters. To illustrate the power of this comparison, Figure 6 shows a small area of the southern galactic cap from both surveys, where extended features in common are highlighted with green arrows. Since the observing strategies, data analysis pipelines, and reddening maps used are all different and independent, the coincidence of these features indicates that they are most likely real. However, we have checked that even the most significant of these features are too faint and/or diffuse to produce convincing CMDs, and therefore we are unable to determine their physical properties with any of the extant data.

That the Milky Way halo may be composed of a myriad of faint tidal streams, most of which lie just below the detection limits of current photometric surveys, is a tantalizing prospect that has also been recently hinted at from spectroscopy (e.g. [Schlaufman et al. 2012](#), and references therein). If confirmed, this would give strong support for the hierarchical model of structure formation on the scale of individual galaxies. Understanding the origins of halo streams is of tantamount importance. Many of the features identified so far are narrow and composed of ancient metal-poor populations, properties that are most consistent with dis-

rupted globular clusters. This suggests that a non-negligible fraction of the stellar halo may have originated in globular clusters, in agreement with chemical tagging analyses (e.g. [Martell et al. 2011, 2016](#); [Ramírez, Meléndez, & Chanamé 2012](#); [Lind et al. 2015](#); [Fernandez-Trincado et al. 2016](#)). The next decade is likely to be pivotal for disentangling the actual make-up and assembly history of the Milky Way halo, with forthcoming wide-field surveys such as the *Large Synoptic Survey Telescope* ([Tyson 2002](#)) reaching several magnitudes beyond what is currently available. In addition, the soon availability of *Gaia* astrometric data will provide crucial constraints on the distances and orbits of nearby streams, as well as facilitate the discovery of new substructures through joint photometric and kinematic searches.

ACKNOWLEDGEMENTS

The authors are grateful to Ana Bonaca for granting us permission to use part of her maps in this publication, and to Jorge Peñarrubia and the anonymous referee for useful comments. EJB acknowledges support from a consolidated grant from STFC and from the CNES postdoctoral fellowship program. HWR acknowledges support from the DFG grant SFB 881 (A3). RFGW acknowledges support through a Visiting Professorship from the Leverhulme Trust, held at the University of Edinburgh. This research work has made use of the Python packages Numpy⁴ ([Walt, Colbert, & Varoquaux](#)

⁴ <http://www.numpy.org/>

2011), Astropy⁵ (Astropy Collaboration et al. 2013), Matplotlib⁶ (Hunter 2007), and Pandas⁷ (McKinney 2010); the IAC-STAR Synthetic CMD computation code, which is supported and maintained by the computer division of the Instituto de Astrofísica de Canarias; and the NASA/IPAC Extragalactic Database which is operated by the Jet Propulsion Laboratory, California Institute of Technology, under contract with the National Aeronautics and Space Administration.

The PS1 Surveys have been made possible through contributions of the Institute for Astronomy, the University of Hawaii, the Pan-STARRS Project Office, the Max-Planck Society and its participating institutes, the Max Planck Institute for Astronomy, Heidelberg and the Max Planck Institute for Extraterrestrial Physics, Garching, The Johns Hopkins University, Durham University, the University of Edinburgh, Queen's University Belfast, the Harvard-Smithsonian Center for Astrophysics, the Las Cumbres Observatory Global Telescope Network Incorporated, the National Central University of Taiwan, the Space Telescope Science Institute, the National Aeronautics and Space Administration under Grant No. NNX08AR22G issued through the Planetary Science Division of the NASA Science Mission Directorate, the National Science Foundation under Grant No. AST-1238877, and the University of Maryland.

REFERENCES

- Aparicio A., Gallart C., 2004, *AJ*, 128, 1465
 Astropy Collaboration, et al., 2013, *A&A*, 558, A33
 Balbinot E., et al., 2013, *ApJ*, 767, 101
 Balbinot E., et al., 2016, *ApJ*, 820, 58
 Belokurov V., Evans N. W., Irwin M. J., Hewett P. C., Wilkinson M. I., 2006a, *ApJ*, 637, L29
 Belokurov V., et al., 2006b, *ApJ*, 642, L137
 Belokurov V., et al., 2007a, *ApJ*, 657, L89
 Belokurov V., et al., 2007b, *ApJ*, 658, 337
 Belokurov V., Koposov S. E., 2016, *MNRAS*, 456, 602
 Bernard E. J., et al., 2014a, *MNRAS*, 443, L84
 Bernard E. J., et al., 2014b, *MNRAS*, 442, 2999
 Bonaca A., Geha M., Kallivayalil N., 2012, *ApJ*, 760, L6
 Bressan A., Marigo P., Girardi L., Salasnich B., Dal Cero C., Rubele S., Nanni A., 2012, *MNRAS*, 427, 127
 Carraro G., Zinn R., Moni Bidin C., 2007, *A&A*, 466, 181
 Crnojević D., et al., 2016, *ApJ*, 823, 19
 Duc P.-A., et al., 2015, *MNRAS*, 446, 120
 Duffau S., Zinn R., Vivas A. K., Carraro G., Méndez R. A., Winnick R., Gallart C., 2006, *ApJ*, 636, L97
 Errani R., Peñarrubia J., Tormen G., 2015, *MNRAS*, 449, L46
 Fernandez-Trincado J. G., et al., 2016, *ApJ*, in press (astro-ph/1604.01279)
 Finkbeiner D. P., et al., 2016, *ApJ*, 822, 66
 Frebel A., Lunnan R., Casey A. R., Norris J. E., Wyse R. F. G., Gilmore G., 2013, *ApJ*, 771, 39
 Geha M., Willman B., Simon J. D., Strigari L. E., Kirby E. N., Law D. R., Strader J., 2009, *ApJ*, 692, 1464
 Girardi L., Bressan A., Bertelli G., Chiosi C., 2000, *A&AS*, 141, 371
 Gómez F. A., White S. D. M., Marinacci F., Slater C. T., Grand R. J. J., Springel V., Pakmor R., 2016, *MNRAS*, 456, 2779
 Grillmair C. J., 2006a, *ApJ*, 645, L37
 Grillmair C. J., 2006b, *ApJ*, 651, L29
 Grillmair C. J., Dionatos O., 2006a, *ApJ*, 641, L37
 Grillmair C. J., Dionatos O., 2006b, *ApJ*, 643, L17
 Grillmair C. J., Carlin J. L., Majewski S. R., 2008, *ApJ*, 689, L117
 Grillmair C. J., 2009, *ApJ*, 693, 1118
 Grillmair C. J., 2011, *ApJ*, 738, 98
 Grillmair C. J., Cutri R., Masci F. J., Conrow T., Sesar B., Eisenhardt P. R. M., Wright E. L., 2013, *ApJ*, 769, L23
 Grillmair C. J., 2014a, *ApJ*, 790, L10
 Grillmair C. J., 2014b, *IAUS*, 298, 405
 Grillmair C. J., Hetherington L., Carlberg R. G., Willman B., 2015, *ApJ*, 812, L26
 Grillmair C. J., Carlberg R. G., 2016, *ApJ*, 820, L27
 Grillmair C. J., Carlin J. L., 2016, in Carlin J. L., Newberg H. J., eds., *Tidal Streams in the Local Group and Beyond: Observations and Implications*, Springer-Verlag
 Harris W. E., 1996, *AJ*, 112, 1487
 Hernitschek N., et al., 2016, *ApJ*, 817, 73
 Hunter J. D., 2007, *Computing In Science & Engineering*, 9, 90
 Ibata R. A., Gilmore G., Irwin M. J., 1994, *Natur*, 370, 194
 Ibata R., Irwin M., Lewis G., Ferguson A. M. N., Tanvir N., 2001, *Natur*, 412, 49
 Ibata R. A., Lewis G. F., Irwin M. J., Quinn T., 2002, *MNRAS*, 332, 915
 Ibata R. A., et al., 2014, *ApJ*, 780, 128
 Ibata R. A., Lewis G. F., Martin N. F., 2016, *ApJ*, 819, 1
 Ivezić Ž., et al., 2000, *AJ*, 120, 963
 Johnston K. V., Hernquist L., Bolte M., 1996, *ApJ*, 465, 278
 Juric M., 2012, *Astrophysics Source Code Library*, record ascl:1209.003
 Koposov S. E., Rix H.-W., Hogg D. W., 2010, *ApJ*, 712, 260
 Koposov S. E., Irwin M., Belokurov V., Gonzalez-Solares E., Yoldas A. K., Lewis J., Metcalfe N., Shanks T., 2014, *MNRAS*, 442, L85
 Lind K., et al., 2015, *A&A*, 575, L12
 Malin D., Hadley B., 1997, *PASA*, 14, 52
 Majewski S. R., Ostheimer J. C., Rocha-Pinto H. J., Patterson R. J., Guhathakurta P., Reitzel D., 2004, *ApJ*, 615, 738
 Martell S. L., Smolinski J. P., Beers T. C., Grebel E. K., 2011, *A&A*, 534, A136
 Martell S. L., et al., 2016, *ApJ*, 825, 146
 Martin N. F., Ibata R. A., Irwin M., 2007, *ApJ*, 668, L123
 Martin N. F., et al., 2014, *ApJ*, 787, 19
 Martínez-Delgado D., et al., 2010, *AJ*, 140, 962
 McKinney, W., 2010, in van der Walt, S. & Millman, J., eds., *Proceedings of the 9th Python in Science Conference*, SciPy, 51
 Morganson E., et al., 2016, *ApJ*, 825, 140
 Newberg H. J., et al., 2002, *ApJ*, 569, 245
 Newberg H. J., Yanny B., Willett B. A., 2009, *ApJ*, 700, L61
 Ngan W., Carlberg R. G., Bozek B., Wyse R. F. G., Szalay A. S., Madau P., 2016, *ApJ*, 818, 194
 Niederste-Ostholt M., Belokurov V., Evans N. W., Gilmore G., Wyse R. F. G., Norris J. E., 2009, *MNRAS*, 398, 1771
 Norris J. E., Wyse R. F. G., Gilmore G., Yong D., Frebel A., Wilkinson M. I., Belokurov V., Zucker D. B., 2010, *ApJ*, 723, 1632
 Odenkirchen M., et al., 2001, *ApJ*, 548, L165
 Odenkirchen M., et al., 2003, *AJ*, 126, 2385
 Odenkirchen M., Grebel E. K., Kayser A., Rix H.-W., Dehnen W., 2009, *AJ*, 137, 3378
 Okamoto S., Arimoto N., Ferguson A. M. N., Bernard E. J., Irwin M. J., Yamada Y., Utsumi Y., 2015, *ApJ*, 809, L1
 Pillepich A., Madau P., Mayer L., 2015, *ApJ*, 799, 184
 Ramírez I., Meléndez J., Chanamé J., 2012, *ApJ*, 757, 164
 Rockosi C. M., et al., 2002, *AJ*, 124, 349

⁵ <http://www.astropy.org>

⁶ <http://matplotlib.org/>

⁷ <http://pandas.pydata.org/>

- Schlafly E. F., et al., 2014, ApJ, 789, 15
Schlafly E. F., Finkbeiner D. P., 2011, ApJ, 737, 103
Schlaufman K. C., Rockosi C. M., Lee Y. S., Beers T. C., Allende Prieto C., Rashkov V., Madau P., Bizyaev D., 2012, ApJ, 749, 77
Sesar B., et al., 2007, AJ, 134, 2236
Sesar B., et al., 2015, ApJ, 809, 59
Shang Z., et al., 1998, ApJ, 504, L23
Shanks T., et al., 2015, MNRAS, 451, 4238
Simon J. D., et al., 2011, ApJ, 733, 46
Slater C. T., et al., 2013, ApJ, 762, 6
Slater C. T., et al., 2014, ApJ, 791, 9
Sollima A., Beccari G., Ferraro F. R., Fusi Pecci F., Sarajedini A., 2007, MNRAS, 380, 781
The Dark Energy Survey Collaboration, 2005, astro-ph/0510346
Tyson J. A., 2002, in Tyson J. A. & Wolf S., eds., Survey and Other Telescope Technologies and Discoveries, Proc. SPIE, 4836, 10
Walt, S. v. d., Colbert, S. C., & Varoquaux, G. 2011, Comp. Sci. Engg., 13, 22
Willman B., et al., 2005a, AJ, 129, 2692
Willman B., et al., 2005b, ApJ, 626, L85
Xu Y., Newberg H. J., Carlin J. L., Liu C., Deng L., Li J., Schönrich R., Yanny B., 2015, ApJ, 801, 105
York D. G., et al., 2000, AJ, 120, 1579